OPTICAL OBSERVATION, IMAGE-PROCESSING, AND DETECTION OF SPACE DEBRIS IN GEOSYNCHRONOUS EARTH ORBIT

Hiroshi ODA, Toshifumi YANAGISAWA, Hirohisa KUROSAKI
Japan Aerospace Exploration Agency, 7-44-1 Jindaiji, Higashimachi, Chofu, Tokyo 182-8522, Japan
Makoto TAGAWA
Kyushu University, 6-10-1 Hakozaki, Higashi-ku, Fukuoka 812-8581, Japan

ABSTRACT

We report on optical observations and an efficient detection method of space debris around the geosynchronous Earth orbit (GEO). We operate our new Australia Remote Observatory (ARO) where an 18 cm optical telescope with a charged-coupled device (CCD) camera covering a 3.17-degree field of view is used for GEO debris survey, and analyze datasets of successive CCD images using the uniform linear motion detection method. In our operation, the exposure time of each CCD image is set to be 3 seconds, and the time interval of CCD shutter open is about 4.7 seconds. In the uniform linear motion detection method, a sufficient number of object candidates is taken from each image based on their shape and intensity, which includes not only faint signals but also background noise. We select 500 object candidates from each image in this paper (the number depends on the limit of computational resources). Then we search a sequence of sample objects showing the uniform linear motion in the successive 18 images. As a result, we detected about 300 GEO objects up to magnitude of 15 among 5 night data. We also identified the objects from the two-line-element (TLE) data catalogue publicly provided by the U.S. Strategic Command (USSTRATCOM). We found that a certain amount of the detected objects are not listed in the catalogue. We conclude that our ARO and detection method posse a high efficiency detection of GEO objects despite the use of comparatively inexpensive observation and analysis system.

We also describe the image-processing specialized for the detection of GEO objects (not for usual astronomical objects like stars) in this paper.

1. INTRODUCTION

One of the most important and valuable orbit around the Earth is the Geosynchronous Earth Orbit (GEO). Now a lot of space debris has been put into the GEO. The U.S. Strategic Command (USSTRATCOM) catalogues objects more than about 1 m in size around GEO and provides orbital information in the NASA two-line-element (TLE) format. The population of fragmented object generated by collisions of space debris is thought to increases with decreasing their size (the mean magnitude or intensity is roughly proportional to their size). However, information on GEO objects less than about 1 m in size, which also can damage spacecraft, is sparse [1].

In the GEO survey, a wide Field-Of-View (FOV) is required in terms of detection efficiency and detection of fast objects. A small telescope with the short focal length has a wide FOV, while the light-gathering power is low in general. However, such an optical system also has the advantage of the long duration time that moving objects stay within a pixel. Although it is difficult to detect a faint GEO object whose intensity is low (comparable to the sky background) from an image, a detection algorithm utilizing successive multiple images can improve the detection limit for such faint objects [2].

We started to operate our new optical observation facility, Australia Remote Observatory (ARO), since 2013, and conduct optical survey for GEO objects. In this paper, we report results of the first year observation at ARO. We also describe image-processing and detection algorithm.

2. OBSERVATIONS

The ARO is located at 27°25′52″S, 151°43′08″E, and altitude of 406 m. We set up an 18 cm optical telescope (the focal length is 500 mm) equipped with a back-illuminated CCD camera (the array size is 2048×2048 and the pixel size is 13.5 μm) covering a 3.17-degree FOV (Fig. 1). We employ the horizontal coordinate system in GEO survey, in which the stars move horizontally in an image, while GEO objects are relatively stationary. In our operation, the exposure time of a light frame is set to be 3 seconds so that typical GEO objects stay in about one

pixel in the exposure. The time interval of CCD shutter open is about 4.7 seconds (sum of the exposure time and data transfer time). We also take a matching frame of 1-second exposure time so that stars appear point-like just before taking the light frames. The matching frame is used for matching the pixel and celestial coordinates of the guide stars. A dataset of an observation region consists of a matching frame and 18 successive light frames.

In this paper, we report on analysis results of 206 dataset observed at the ARO on the five night of 2013 June 7, 11, August 8, November 1, and 6.

Fig. 1. Left: The perspective of the sky from the sliding roof of ARO. Top-right: The 3m sliding roof. Bottom-right: The 18 cm telescope and back-illuminated CCD camera.

3. IMAGE-PROCESSING

We subtract a master dark-bias frame (a median combining of 16 dark-bias frames) from raw images to minimize the dark current noise, and divide the images by a master flat-field frame to correct for variation in the sensitivity of pixels and uneven illumination (Fig. 2. second panel). Here we use a sky flat-field frame whose maximum intensity is about 30 percent of the full saturation level of the CCD chip. In the sky background subtraction, we first create a rough estimate of the sky background by applying a median filter to a median combining of 18 light frames. Then, we mask bright pixels in the light frame substituting values on relevant pixels of the rough estimate into the selected pixels. To create a sky background frame, we smooth the masked image by applying a uniform filter to it. Finally, we subtract the sky background frame from the light frame (Fig. 2. third panel).

For the convenience in the detection of GEO objects, we mask the diurnal motion objects (stars) utilizing the next observation time step image. The travel distance of stars due to the diurnal motion can be computed precisely. In our optical system, a star streak of about 8 pixels appears in a light frame (3 seconds exposure). The travel distance of the star streak due to the diurnal motion is roughly 13 pixels for about 4.7 seconds time interval. We mask the star streaks in the current light frame utilizing the next light frame. We first select bright pixels whose value exceed a threshold derived from the sigma-clipped mean and deviation in the next light frame, and expand the selected pixel aria by 2 or 3 pixels (marginal pixels) to completely mask star streaks region. We shift these pixels by the travel distance in the opposite direction to the diurnal motion, and overlay the shifted pixels on the current image. Then, we substitute the rough estimate value of sky background into the shifted pixels to mask the star streaks in the current light frame (Fig. 2. bottom panel). We note that, for the last successive light frame, we use the previous light frame instead of the next light frame.

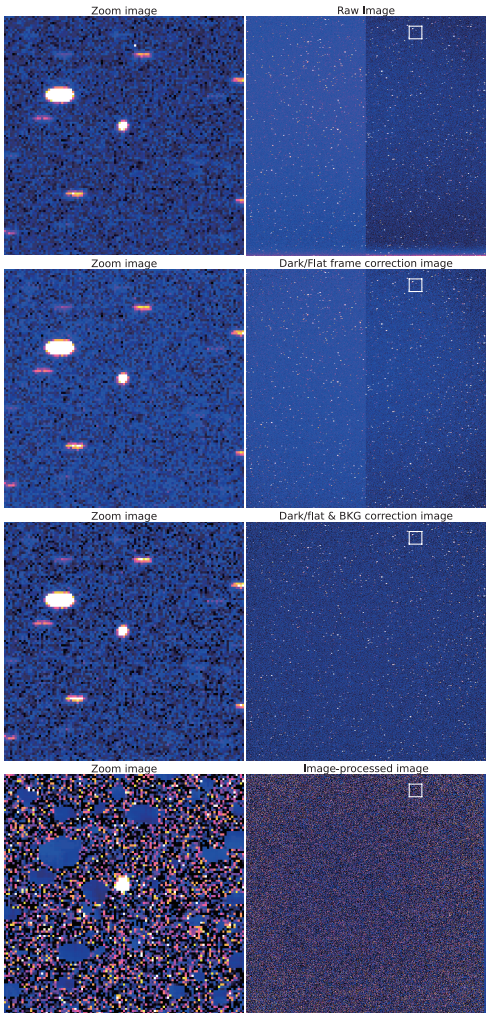

Fig. 2. Example of image-processing at the raw image (top), dark-bias frame subtraction and flat-field frame correction (second), background subtraction (third), and diurnal motion masking (bottom). Right: Whole image. Left: Zoomed image of white rectangle in the right panels.

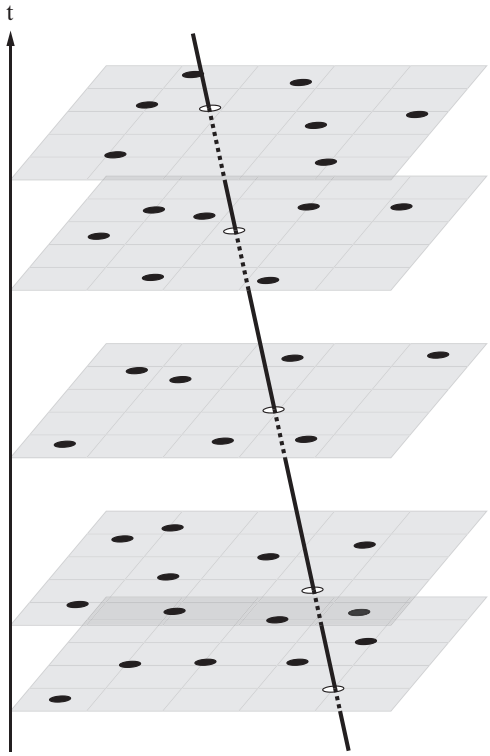

Fig. 3. Concept of the uniform linear motion detection algorithm.

4. DETECTION ALGORITHM

We apply the uniform linear motion detection algorithm [2] to the 18 successive light frames in order to improve the detection limit for faint objects whose intensities are comparable with that of the sky background noise. The concept of the algorithm is to search objects showing the uniform linear motion in the successive light frame (Fig. 3). The path of orbital object can be regarded as the uniform linear motion in a sufficiently narrow FOV compared to the whole orbital path. At the first step, we select candidates of moving objects in each light frame based on their intensity and shape (diffusive object image). The photon flux from an orbital object is spread over several pixels due to the atmospheric turbulence. For this reason, the shape of orbital object in an image is diffusive. On the other hand, the shape of noise tends to be point-like. At the next step, we search objects showing the uniform linear motion among these candidates to exclude the noise and cosmic rays that appear randomly (do not show the uniform linear motion). In this analysis, we select the brightest 500 candidates satisfying the selection condition of shape in each light frame, and consider the object showing the uniform linear motion (to a tolerance of 2 pixels) in more than 9 light frames out of 18 light frames as the orbital object.

5. PHOTOMETORY AND POSITION DTERMINATION

The pixel selected in the uniform linear motion detection algorithm is just the pixel at the peak intensity but not the precise center position that is required to identify the object from a catalogue. We fit the two-dimensional Gaussian function in order to determine the precise center position and to calculate the total intensity. In the calculation of the total intensity, we sum pixel values greater than the value at 3 σ, where σ is the Gaussian RMS width (Fig. 4). We note that the calculated intensity of a faint object may not be correct because the intensity is comparable with the standard deviation of the sky background (roughly 25 [ADU] in the data analyzed in this paper).

We match the pixel and celestial coordinates and conduct photometry utilizing the Image Reduction and Analysis Facility (IRAF). First, we perform dark-bias frame subtraction, flat-field frame correction, and sky background subtraction to a matching frame of 1-second exposure time (taken just before 18 light frames) in the same way for the light frames. Next, we detect about 100 sample star objects from the matching frame, and match the pixel and celestial coordinates referring the Guide Star Catalogue. In addition, we also compute the plate solutions. Finally, we transform coordinates of the detected objects from the pixel to celestial coordinates applying the plate solutions. Here, we consider the diurnal motion in accordance with the time interval between a matching frame and each light frame. Using the right ascension and declination computed here, we try to identify the detected object from the two-line-element (TLE) data catalogue publicly provided by the U.S. Strategic Command (USSTRATCOM).

We also conduct photometry for the sample star objects in order to estimate the magnitude of the detected objects. The pixel intensity of the sample star object is associated with the magnitude referred in the Guide Star Catalogue. Using the relation between the intensity and magnitude of sample stars, we estimate the magnitude of the detected object.

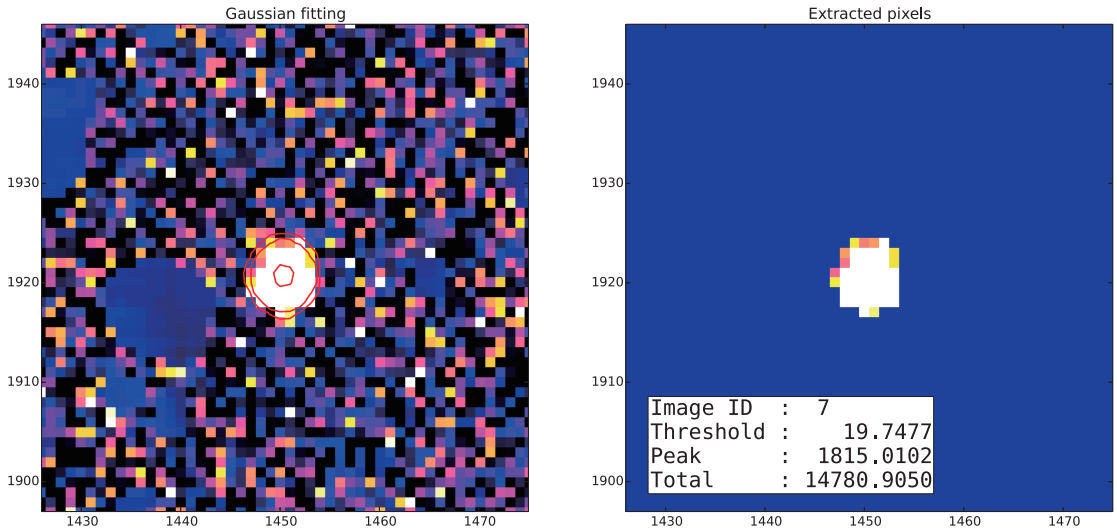

Fig. 4. Left: Example of the two dimensional Gaussian fitting to the cropped data array. The red lines represent the contour plot of 1σ, 3σ, and 3.5σ, respectively, where σ is the Gaussian RMS width. Right: The extracted pixels whose values are greater than 3σ inside the region surrounded by the contour line of 3.5σ.

6. RESULTS

We detected 289 objects in the 5 night data obtained at the ARO on 2013/06/07, 06/11, 08/08, 11/01, and 11/06. Fig. 5 shows an example of the bright object (the mean magnitude is 11.79) detected in the region 27 on 2013/08/08, which is identified as EKRAN 8 13056U 82009A. Fig. 6 shows an example of the faint object (the mean magnitude is 15.11) detected in the region 49 on 2013/11/01, which is not identified. We succeeded in detection of such a faint object. However, we note that the magnitude of such a faint object may not be correct because the pixel intensity is comparable to the sky background. Fig. 7 shows an example of the fast object detected in the region 58 on 2013/11/01 (identified as MERIDIAN 2 35008U 09029A). The velocity is 21.85 [pix/sec] ~

0.034 [deg/sec]. Since this object may be an MEO object, the apparent velocity could be so high if we observed it around the perigee. Fig. 8 shows an example of the periodic intensity oscillation object detected in the region 23 on 2013/11/01. Although the observation time is a little too short to determine the oscillation period precisely, this light curve suggests that the object is rotating.

Fig. 9 shows the magnitude-number distribution of the detected objects. We note again that the photometry therefore number distribution may not correct around the magnitude of 15 because the pixel intensity is comparable to the sky background. The sensitivity limit of this observation system is around there. Fig. 10 shows the same magnitude-number distribution as Fig. 9 but the identified objects and not-identified objects are represented by the blue and green bar, respectively. We found that about one third of the detected objects is not identified.

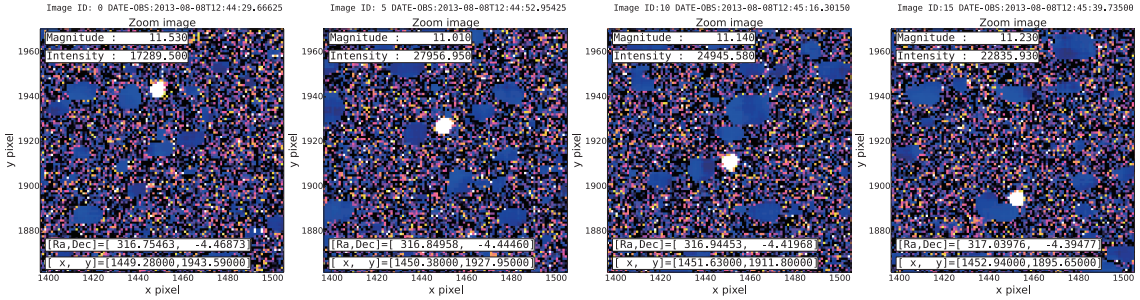

Fig. 5. Example of the bright object detected in the region 27 on 2013/08/08. The mean magnitude is 11.79.

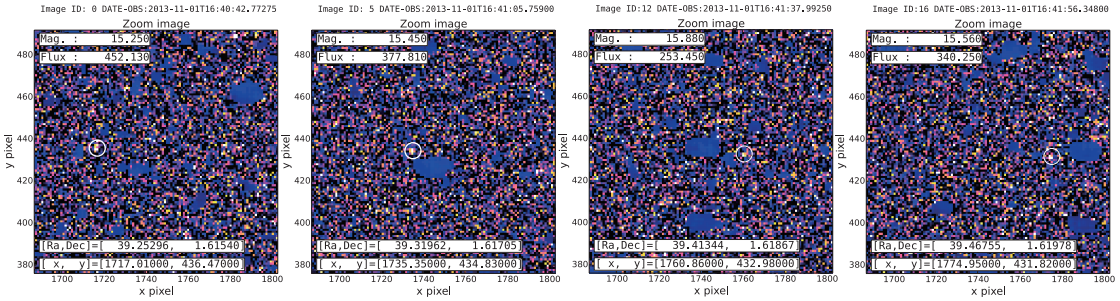

Fig. 6. Example of the faint object detected in the region 49 on 2013/11/01. The object detected in each image is at the center of the white open circle. The mean magnitude is 15.44.

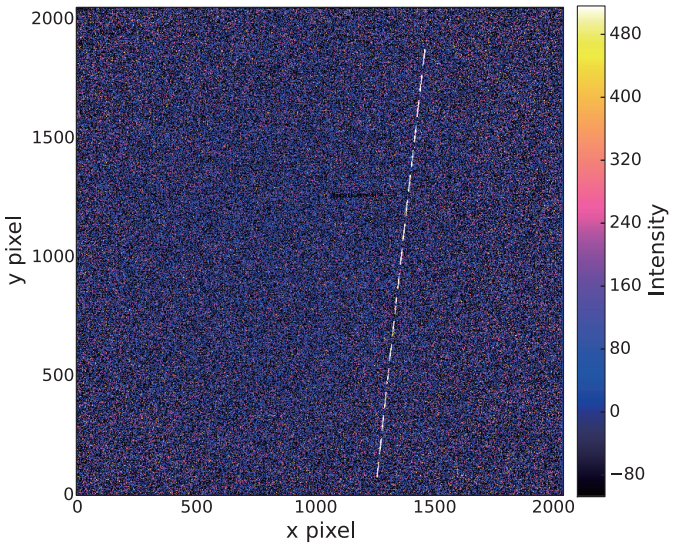

Fig. 7. Example of the fast object detected in the region 58 on 2013/11/01. The mean magnitude is 6.83. The detected object moves from bottom to top in the FOV with the velocity of 21.85[pix/sec] (~ 0.034[deg/sec]).

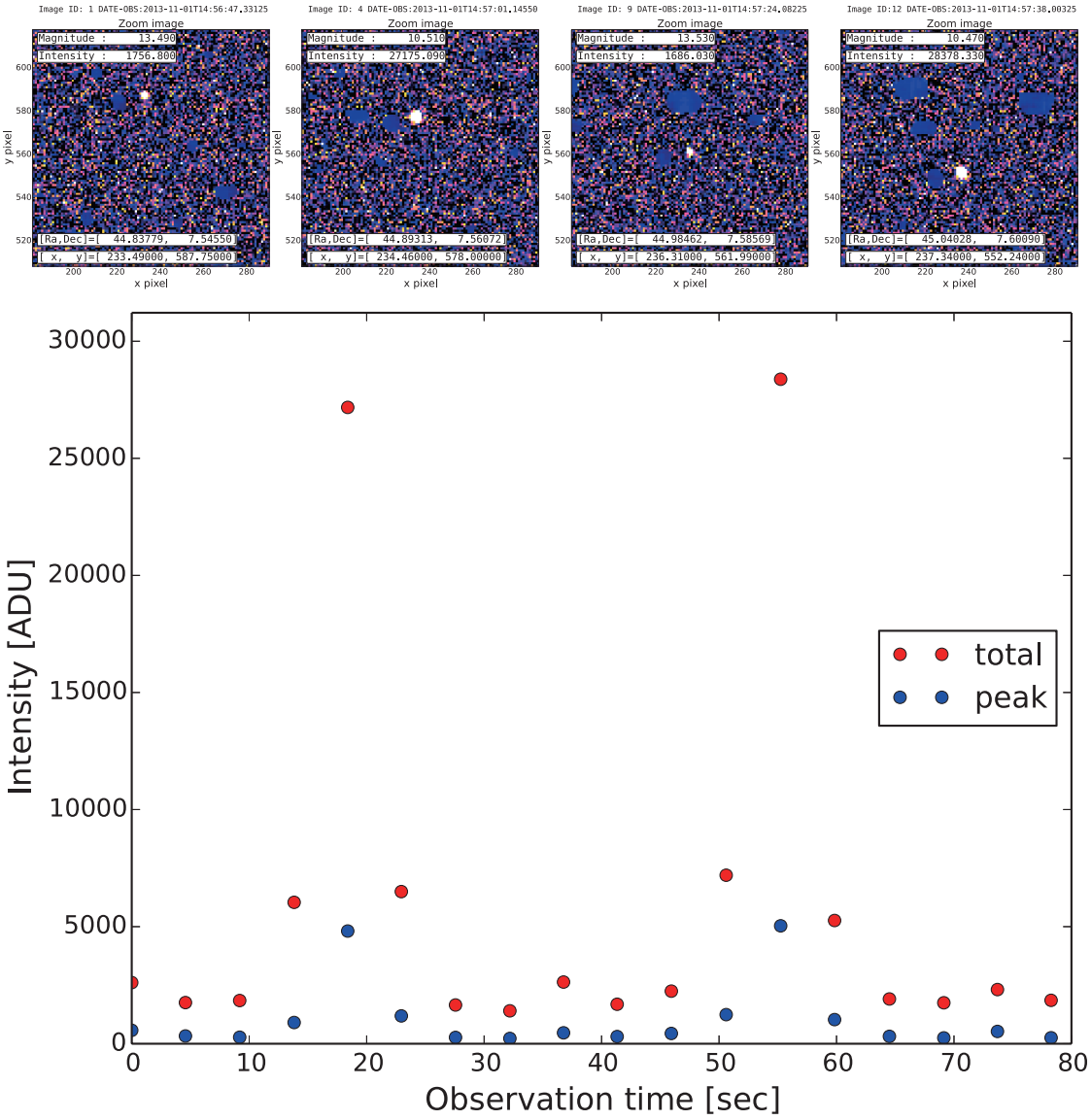

Fig. 8. Example of the periodic intensity oscillation object detected in the region 23 on 2013/11/01. Bottom: Time variation of the total intensity (red) and the peak (maximum pixel value) intensity (blue) of the detected object.

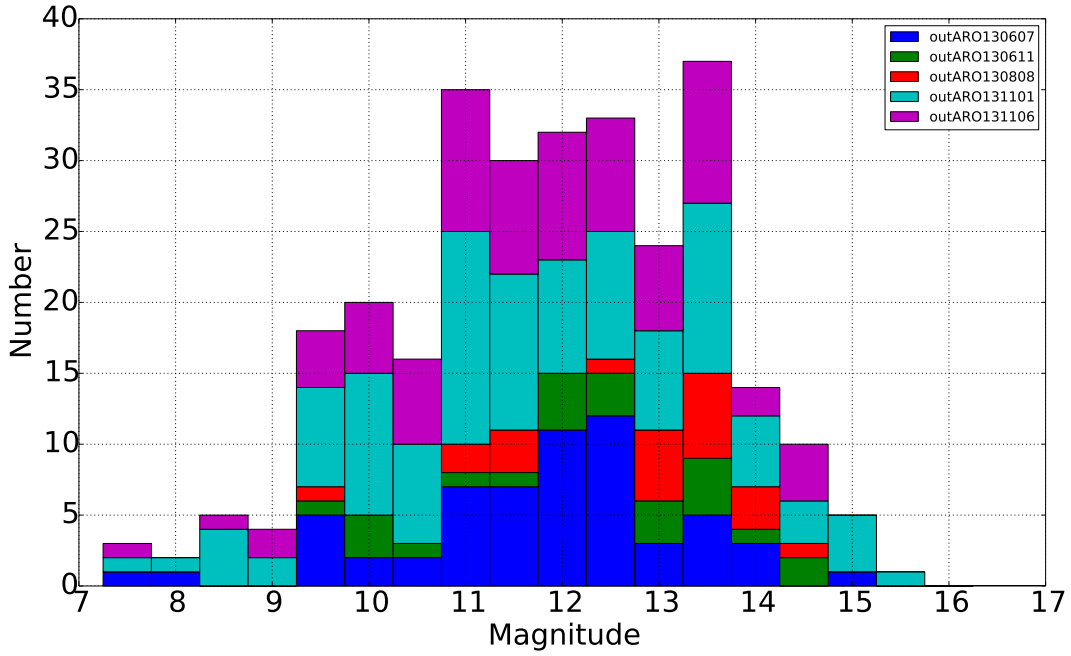

Fig. 9. Magnitude - Number distribution of detected objects in data of 2013 June 7 (blue), 11 (green), August 8 (red), November 1 (cyan), and 6 (purple). The total detection number is 289.

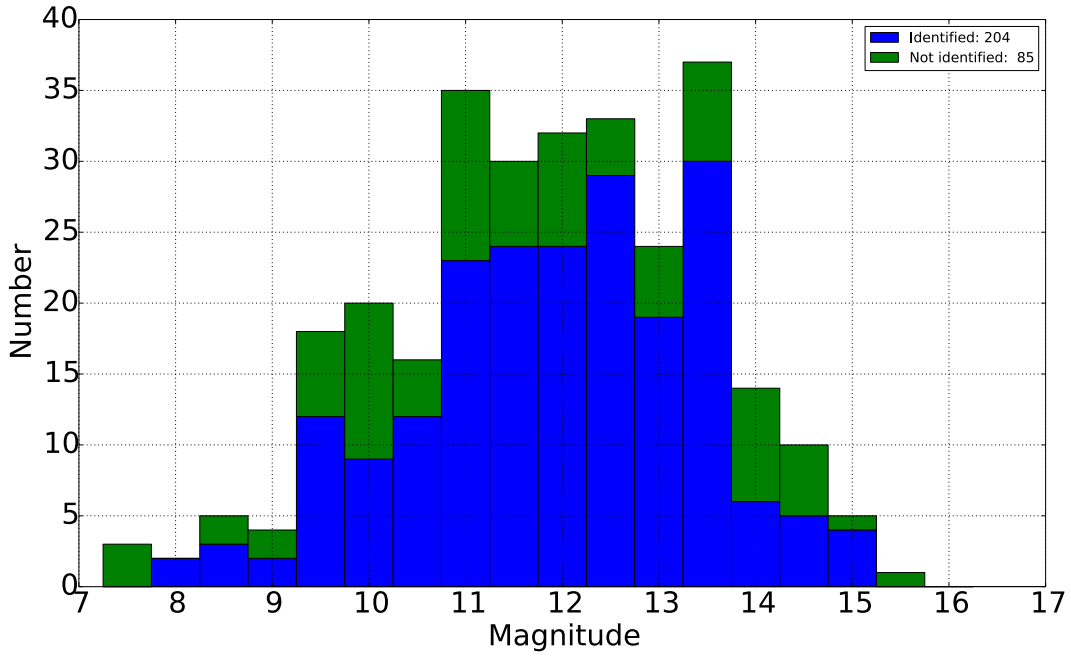

Fig. 10. Same as Fig. 9. but the identified object and not identified object are represented by the blue and green bar, respectively. About one third of the detected objects is not identified.

7. CONCLUSION AND DISCUSSION

We started to operate our new observatory, ARO, since 2013. In this observation site, we used 18 cm optical telescope with CCD, and operated the GEO survey. We applied the uniform linear motion detection algorithm to the successive images. As a result, we detected about 300 objects up to magnitude of 15 from 5 night data. We conclude that ARO posses a good efficiency for detection of GEO objects despite the use of comparatively low-cost and low-sensitive observation system. However, according to the prediction of ESA's PROOF, the number distribution of fragmented objects increases with the magnitude, in particular, in the range of the magnitude greater than about 15. This range is close to the sensitivity limit of the ARO observation system unfortunately. Recently, we replaced the 18 cm telescope with 25 cm telescope to improve the sensitivity limit. In addition, we plan to apply the stacking method [2] as a detection algorithm. In this algorithm, images are shifted along to the possible predicted moving direction and stacked. As a result, the signal from an orbital object is amplified while the noise is reduced relatively. We expect that the detection limit be improved by 2 magnitudes empirically. However, huge computational resources are required because the images must be shifted to the all-possible predicted direction. To solve this problem, we plan to accelerate it by making use of GPU (for instance, NVIDIA Tesla K20). Then, we investigate the number distribution of fainter objects.

8. ACKNOWLEDGEMENTS

We would like to thank Mr. Kazuyuki Tanaka for setup of observational equipment and improvement of networking infrastructure at ARO.

9. REFERENCES

1. Schildknecht, T., Ploner, M., and Hugentobler, U., "The search for debris in GEO", Adv. Space Res. Vol. 28, No. 9, pp. 1291-1299, 2001.
2. Yanagisawa, T., Kurosaki, H., and Nakajima, A.: JAXA's Optical Observation Facility for Space Debris Observation and Its Activities, Trans. JSASS Aerospace Tech. Japan Vol. 8, No. ists27, pp. Pr_2_49-Pr_2_53, 2010.